*Inorg. Chem.* **2009**, *48*, 209−220

# Investigation of the $[Cp^*Mo(PMe_3)_3H]^{n+}$ ($n = 0, 1$) Redox Pair: Dynamic Processes on Very Different Time Scales

**Miguel Baya,[†,‡,§] Pavel A. Dub,[†,||,⊥] Jennifer Houghton,[†] Jean-Claude Daran,[†,⊥] Natalia V. Belkova,[||] Elena S. Shubina,*[,||] Lina M. Epstein,[||] Agustí Lledós,*[,‡] and Rinaldo Poli*[,†,⊥,#]**

*LCC (Laboratoire de Chimie de Coordination), CNRS, 205 route de Narbonne, F-31077 Toulouse, France, Departament de Química, Edifici Cn, Universitat Autónoma de Barcelona, 08193 Bellaterra, Spain, Nesmeyanov Institute of Organoelement Compounds, Russian Academy of Sciences, Vavilov Street 28, 119991 Moscow, Russia, UPS, INP, Université de Toulouse, F-31077 Toulouse, France, and Institut Universitaire de France, 103 bd Saint-Michel, 75005 Paris, France*

Received September 1, 2008

The compound $[Cp^*Mo(PMe_3)_3H]$ (**1**) is reversibly oxidized at $E_{1/2} = -1.40$ V vs ferrocene in MeCN. Its oxidation with $Cp_2FePF_6$ yields thermally stable $[Cp^*Mo(PMe_3)_3H]PF_6$ (**2**), which has been isolated and characterized by IR and EPR spectroscopy and by single-crystal X-ray diffraction. The $^1H$ and $^{31}P$ NMR spectra of **1** show two types of $PMe_3$ ligands in a 1:2 ratio at low temperature, but only one average signal at room temperature, with activation parameters of $\Delta H^{\ddagger} = 11.7(3)$ kcal mol$^{-1}$ and $\Delta S^{\ddagger} = -3(1)$ eu for the exchange process. Although only one species is evidenced by NMR for **1** and by EPR for **2**, the solution IR spectra of each complex show two bands in the $\nu$(Mo−H) region (**1**, major at 1794 cm$^{-1}$ and minor at ca. 1730 cm$^{-1}$; **2**, ca. 1800 and 1770 cm$^{-1}$ with approximately equal intensity), the position and relative intensity being little dependent on the solvent. A thorough DFT investigation suggests that these are different rotamers involving different relative orientations of the Cp* ring and the $PMe_3$ ligands in these complexes. This ring rotation process is very rapid on the NMR and EPR time scale but slow on the IR time scale. The X-ray data and the theoretical calculations suggest the presence of weak Mo−H···F interactions in compound **2**. The possibility of $PMe_3$ dissociation, as well as other intramolecular rearrangements, for **1** and **2** is excluded by experimental and computational studies. Protonation of **1** yields $[Cp^*Mo(PMe_3)_3H_2]^+$ (**3**), which also reveals a dynamic process interconverting the two inequivalent H ligands and the three $PMe_3$ ligands (two sets in a 1:2 ratio in the frozen structure) on the NMR time scale (activation parameters of $\Delta H^{\ddagger} = 9.3(1)$ kcal/mol and $\Delta S^{\ddagger} = -4.1(4)$ eu). A DFT study suggests that this exchange process occurs via a low-energy symmetric dihydride intermediate and not through a dihydrogen complex.

## Introduction

Hydride complexes generally feature a closed-shell configuration. They are implicated in a variety of catalytic cycles and are also intermediates of C−H oxidative addition processes. Open-shell, paramagnetic versions, on the other hand, have not so far demonstrated broad utility, mainly because of their instability and multitude of decomposition pathways, including deprotonation,[1] disproportionation,[2] dihydrogen reductive elimination (for complexes containing at least two hydride ligands),[3] atom transfer, etc.,[4] yet

* To whom correspondence should be addressed. Fax: (+) 33-561553003 (R.P.). E-mail: shu@ineos.ac.ru (E.S.S.), agusti@klingon.uab.es (A.L.), rinaldo.poli@lcc-toulouse.fr (R.P.).
† CNRS.
‡ Universitat Autónoma de Barcelona.
§ Present address: Departamento de Química Inorgánica, Instituto de Ciencia de Materiales de Aragün, Universidad de Zaragoza−CSIC, 50009 Zaragoza, Spain.
|| Russian Academy of Sciences.
⊥ Université de Toulouse.
# Institut Universitaire de France.

(1) Ryan, O. B.; Tilset, M.; Parker, V. D. *J. Am. Chem. Soc.* **1990**, *112*, 2618–2626.
(2) Smith, K.-T.; Rømming, C.; Tilset, M. *J. Am. Chem. Soc.* **1993**, *115*, 8681–8689.
(3) Pleune, B.; Morales, D.; Meunier-Prest, R.; Richard, P.; Collange, E.; Fettinger, J. C.; Poli, R. *J. Am. Chem. Soc.* **1999**, *121*, 2209–2225.
(4) Poli, R. Paramagnetic Mono- and Polyhydrides of the Transition Metals. In *Recent Advances in Hydride Chemistry*; Poli, R., Peruzzini, M., Eds.; Elsevier Science: Amsterdam, 2001; pp 139−188.

10.1021/ic801676n CCC: $40.75 
Published on Web 12/05/2008

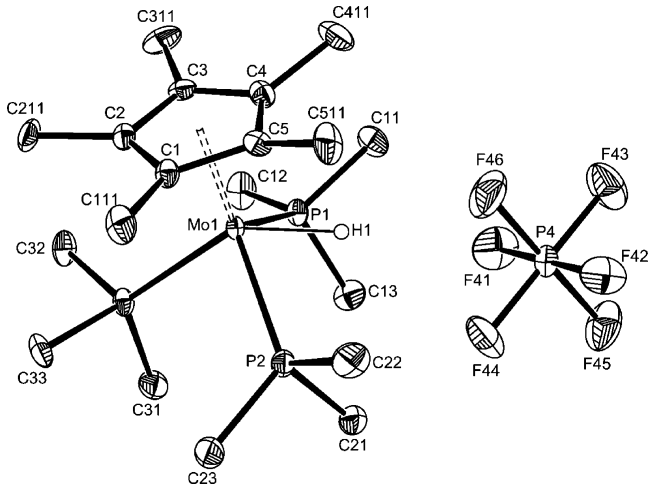


**Figure 1.** An ORTEP view of compound **2** (ellipsoids are drawn at the 30% probability level). All hydrogen atoms except the hydride are not shown for clarity.

fundamental processes such as dihydrogen evolution in nature appear to take place via open-shell hydride complexes.[5−8] It is also possible to imagine potential implication in electrocatalytic hydrocarbon oxidation. Therefore, paramagnetic hydride complexes are attracting renewed interest. It has long been known that one-electron oxidation of hydride complexes increases the M−H bond acidity.[1] However, this property highly depends on the medium.[9,10] For instance, hydride complexes with hydridic character may be strong acids in water.[10]

Many oxidized hydride complexes spontaneously decompose by transferring a proton to a base, which may be the 18-electron hydride precursor itself.[4] Suppression of this reactivity has been achieved by the use of strong donating ligands possessing, at the same time, a significant steric bulk.[11,12] We have previously shown that the electron-rich hydride complex $[CpMo(PMe_3)_3H]$ is reversibly oxidized to yield unstable 17-electron $[CpMo(PMe_3)_3H]^+$,[13] which decomposes by deprotonation and disproportionation at room temperature. We have therefore turned our attention to the bulkier and electron-richer Cp* analogue $[Cp^*MoH(PMe_3)_3]$, **1**.[14] In this paper, we will show that this indeed leads to a more stable one-electron oxidation product, $[Cp^*MoH(PMe_3)_3]^+$, **2**. We present here the synthesis and characterization of this material, including detailed spectroscopic studies, and a computational investigation designed to elucidate the nature of a second product that has been detected in solution for both **1** and **2**.

**Table 1.** Selected Bond Distances (Å) and Angles (deg) for Compound **2** and Comparison with the DFT-Optimized Parameters for the Cation in the Gas Phase[a]

| | exptl (X-ray) | DFT-optimized (cation) | DFT-optimized (cation + anion) |
|---|---|---|---|
| CNT−Mo | 2.0021(6) | 2.067 | 2.071 |
| Mo−H | 1.72(6) | 1.699 | 1.691 |
| Mo−$P_t$ | 2.490(2) | 2.598 | 2.565 |
| Mo−$P_c$ | 2.480(2) | 2.553 | 2.551 |
| Mo−$P_c$ | 2.475(2) | 2.555 | 2.563 |
| CNT−Mo−H | 107(2) | 105.91 | 106.23 |
| CNT−Mo−$P_t$ | 114.66(5) | 116.56 | 116.21 |
| CNT−Mo−$P_c$ | 122.34(5) | 121.16 | 123.26 |
| CNT−Mo−$P_c$ | 121.97(6) | 120.76 | 120.13 |
| H−Mo−$P_t$ | 138(2) | 137.45 | 137.55 |
| H−Mo−$P_c$ | 70(2) | 69.60 | 66.70 |
| H−Mo−$P_c$ | 66(2) | 67.43 | 67.82 |
| $P_t$−Mo−$P_c$ | 88.94(7) | 89.76 | 89.64 |
| $P_t$−Mo−$P_c$ | 89.20(7) | 87.86 | 89.43 |
| $P_c$−Mo−$P_c$ | 109.33(7) | 111.17 | 108.85 |

[a] The subscripts in $P_c$ and $P_t$ refer to the positions *cisoid* and *transoid* to the hydride ligand.

## Results and Discussion

**(a) Synthesis and Characterization of $[Cp^*Mo(PMe_3)_3H]^+PF_6^-$, 2.** A cyclic voltammetric study of **1** shows a reversible oxidation process ($\Delta E_p = 64$ mV; cf. 67 mV for ferrocene under the same conditions) at $E_{1/2} = -1.40$ V vs ferrocene in MeCN (−1.35 V in THF). This should be compared with the reversible oxidation of the analogous Cp compound at $E_{1/2} = -1.46$ V vs ferrocene in MeCN. These low potentials make these complexes stronger reductants than $Cp_2Co$ (for which $E_{1/2} = -1.33$ V vs ferrocene in $CH_2Cl_2$), although not as strong as $Cp^*_2Co$ ($E_{1/2} = -1.94$ V).[15] We are not aware of other hydride complexes with such low $E_{1/2}$ values. Note that the oxidation of **1** is slightly less facile than that of the Cp analogue. This is an unexpected result, because replacement of Cp with the electron-richer Cp* ligand usually causes a considerable negative shift in the oxidation potential. The reason for this trend reversal is unclear and is still under investigation. In line with our expectations (see the Introduction), however, the one-electron oxidation product **2**, generated by oxidation of $[Cp^*Mo(PMe_3)_3H]$ with 1 equiv of $Cp_2FePF_6$ in THF (see eq 1), is thermally more stable than the Cp analogue. It is moderately stable in MeCN at room temperature, decomposing slowly over a period of 24 h and could be crystallized by slow diffusion of either diethyl ether or pentane into a THF solution at −40 °C to yield suitable single crystals for an X-ray analysis. In the solid state, the compound does not significantly deteriorate upon standing in air at room temperature, in contrast to the extreme air sensitivity of its precursor **1**. A view of the molecule is shown in Figure 1. Relevant bonding parameters are collected in Table 1. The coordination geometry around the Mo atom is

(5) Foerster, S.; Stein, M.; Brecht, M.; Ogata, H.; Higuchi, Y.; Lubitz, W. *J. Am. Chem. Soc.* **2003**, *125*, 83–93.
(6) Igarashi, R. Y.; Laryukhin, M.; Dos Santos, P. C.; Lee, H.-I.; Dean, D. R.; Seefeldt, L. C.; Hoffman, B. M. *J. Am. Chem. Soc.* **2005**, *127*, 6231–6241.
(7) Gloaguen, F.; Lawrence, J. D.; Rauchfuss, T. B. *J. Am. Chem. Soc.* **2001**, *123*, 9476–9477.
(8) Mejia-Rodriguez, R.; Chong, D. S.; Reibenspies, J. H.; Soriaga, M. P.; Darensbourg, M. Y. *J. Am. Chem. Soc.* **2004**, *126*, 12004–12014.
(9) Kristjánsdóttir, S. S.; Norton, J. R. Acidity of Hydrido Transition Metal Complexes in Solution. In *Transition Metal Hydrides*; Dedieu, A., Ed.; VCH: New York, 1992; pp 309−359.
(10) Jacobsen, H.; Berke, H. Hydridicity of Transition Metal Hydrides and Its Implications for Reactivity. In *Recent Advances in Hydride Chemistry*; Poli, R., Peruzzini, M., Eds.; Elsevier Science: Amsterdam, 2001; pp 89−116.
(11) Baya, M.; Houghton, J.; Daran, J.-C.; Poli, R. *Angew. Chem., Int. Ed.* **2007**, *46*, 429–432.
(12) Baya, M.; Houghton, J.; Daran, J.-C.; Poli, R.; Male, L.; Albinati, A.; Guttman, M. *Chem.−Eur. J.* **2007**, *13*, 5347–5359.
(13) Fettinger, J. C.; Kraatz, H.-B.; Poli, R.; Quadrelli, E. A.; Torralba, R. C. *Organometallics* **1998**, *17*, 5767–5775.
(14) Abugideiri, F.; Kelland, M. A.; Poli, R.; Rheingold, A. L. *Organometallics* **1992**, *11*, 1303–1311.
(15) Connelly, N. G.; Geiger, W. E. *Chem. Rev.* **1996**, *96*, 877–910.

that of a typical four-legged piano stool. The hydride H atom was directly located from difference Fourier maps and freely refined. Although the Mo−H distance of 1.72(6) Å is not very accurately determined, it corresponds closely to the Mo−H distances determined by neutron diffraction for other molybdenum hydride compounds: 1.685(3) Å for $Cp_2MoH_2$,[16] 1.69(5) Å for Mo(H)($\eta^2$-Me$_2$C═NAr)[N*i*Pr(3,5-C$_6$H$_3$Me$_2$)]$_2$,[17] 1.712(8), 1.719(9), and 1.719(9) Å for (1,2,4-C$_5$H$_2$*i*Bu$_3$)Mo(PMe$_3$)$_2$H$_3$,[12] and 1.789(7) Å for Cp*Mo(CO)$_3$H.[18]

$$[Cp^*Mo(PMe_3)_3H] + Cp_2FePF_6 \rightarrow Cp_2Fe + [Cp^*Mo(PMe_3)_3H]^+PF_6^- \quad (1)$$

One interesting structural feature is the relative location of the two ions, with the $PF_6^-$ ion facing the cation on the same side as the hydride ligand. Since the oxidation of hydride complexes is known to often induce decomposition by deprotonation,[4] this observation suggests that the hydride ligand has become polarized $\delta+$ and that it establishes a Coulombic interaction with the $PF_6^-$ anion. The H···F distances are quite long (3.33, 3.56, and 3.58 Å) for consideration as hydrogen bonds, but the $PF_6^-$ ion is prevented from more closely approaching the hydride ligand by contacts with a number of Cp* and PMe$_3$ H atoms (see Figure S1 in the Supporting Information, the shortest contacts being F41···H11A, 2.80 Å, F44···H21D, 2.50 Å, and F46···H51A, 2.85 Å). For other previously described cationic paramagnetic hydride complexes, for instance [Cp*W(dppe)H$_3$]$^+$PF$_6^-$,[3] [(1,2,4-C$_5$H$_2$*t*Bu$_3$)Mo(PMe$_3$)$_2$H$_3$]$^+$-PF$_6^-$,[11] and [(1,2,4-C$_5$H$_2$*t*Bu$_3$)Mo(PMe$_3$)$_2$H]$^+$PF$_6^-$,[11] no significant contacts were observed between the anion and the hydride ligand(s). The question of the charge on the hydride ligand in this compound has been addressed by computational methods (vide infra).

In agreement with the presence of a single unpaired electron, solutions of complex [Cp*Mo(PMe$_3$)$_3$H]$^+$ in THF are EPR active. However, the isotropic spectrum is rather broad (width 274 G at 273 K) and does not reveal any hyperfine structure, in contrast to the sharp EPR spectrum of the Cp analogue.[13] Cooling the sample does not result in any significant sharpening down to the freezing point. A frozen glass spectrum exhibits an essentially cubic tensor and is much sharper (width 21.3 G at 110 K) than the isotropic spectrum, but insufficiently so to reveal any hyperfine coupling. Figures of these spectra are available as Supporting Information (Figures S2 and S3). Whereas the neutral precursor is unstable in $CH_2Cl_2$ solution, leading to hydride transfer to the solvent and formation of Cp*Mo-(PMe$_3$)$_3$Cl,[19] the oxidized complex is stable under the same conditions. This is in line with the expected hydridicity reduction upon oxidation.

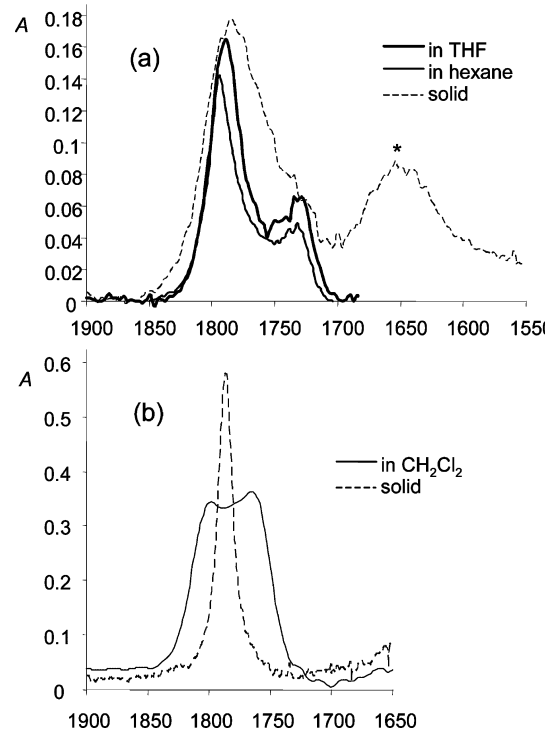


**Figure 2.** Infrared spectra of (a) the complex Cp*Mo(PMe$_3$)$_3$H (0.08 M, 0.4 mm path length) at room temperature (thinner line, in hexane; thicker line, in THF) and (b) the complex [Cp*Mo(PMe$_3$)$_3$H]PF$_6$ (0.042 M, 1.2 mm path length) in $CH_2Cl_2$ at 200 K. The band labeled with an asterisk in (a) is due to an oxidation impurity (see the text).

**(b) Infrared Characterization of Complexes 1 and 2.** The ground-state properties of the Mo−H bond for the neutral and cationic complexes were probed by infrared spectroscopy in solution (Figure 2). An immediately striking observation is the presence of two bands in each case, whereas only one band is expected for a monohydride complex. A major band around 1794 cm$^{-1}$ and a minor one at ca. 1730 cm$^{-1}$ are observed in both *n*-hexane and THF for **1**, whereas two bands of approximately equal intensity at ca. 1800 and 1770 cm$^{-1}$ are observed in both THF and $CH_2Cl_2$ for the cationic complex **2**. The observed blue shift upon oxidation parallels that reported for other redox couples, for instance, [CpFeH(dippe)]$^{0/\bullet+}$ ($\Delta\nu_{(M-H)} = +28$ cm$^{-1}$) and [Cp*FeH(dippe)]$^{0/\bullet+}$ ($\Delta\nu_{(M-H)} = +14$ cm$^{-1}$).[20] The parallel magnetic resonance investigations (NMR for **1** and EPR for **2**) did not show any evidence for the presence of more than one species in solution. However, the time scale of the magnetic resonance techniques is longer than that of infrared spectroscopy; thus, they may reveal average resonances of rapidly equilibrating species. The alternative possibility that the second band is due to a Fermi resonance appears invalid, at least for compound **1**, by the observation that both bands disappear upon carrying out a H/D exchange at the hydride position. The exchange was quite slow in $CD_3OD$ at room temperature, since the two bands decreased only by a factor of ca. 50% upon stirring overnight, but both decreased by essentially the same factor ($I_{major}/I_{minor} = 2.89$ initially, 2.57 after overnight stirring and 47% conversion), proving that

(16) Schultz, A. J.; Stearley, K. L.; Williams, J. M.; Mink, R.; Stucky, G. D. *Inorg. Chem.* **1977**, *16*, 3303–6.
(17) Tsai, Y.-C.; Johnson, M. J. A.; Mindiola, D. J.; Cummins, C. C. *J. Am. Chem. Soc.* **1999**, *121*, 10426–10427.
(18) Brammer, L.; Zhao, D.; Bullock, R. M.; Mcmullan, R. K. *Inorg. Chem.* **1993**, *32*, 4819–4824.
(19) Abugideiri, F.; Fettinger, J. C.; Keogh, D. W.; Poli, R. *Organometallics* **1996**, *15*, 4407–4416.
(20) Jiménez-Tenorio, M.; Puerta, M. C.; Valerga, P. *Organometallics* **1994**, *13*, 3330–3337.

they belong to two difference hydride species in rapid equilibrium. The corresponding Mo−D stretching vibrations (expected at ca. 1270−1220 $cm^{-1}$) could not be observed because of their very low relative intensity and because many other bands are present in this region of the spectrum. However, positive evidence for the formation of [Cp*Mo($PMe_3$)$_3$D] was obtained by $^2$H NMR, with the observation of a quartet resonance at $\delta$ −5.23 ($^2J_{DP}$ = 7.4 Hz) in ca. 30:70 $C_6D_6$−$CD_3OD$ (cf. $\delta$ −4.88 with $^2J_{HP}$ = 47.5 Hz in the $^1$H NMR under the same conditions).

Contrary to the solution infrared spectra, the solid-state spectra of **1** and **2** do not clearly reveal a second component. In the spectrum of **1** (Figure 2a), the presence of a second low-frequency component is not completely excluded because of the large bandwidth (the band marked with an asterisk centered at 1650 $cm^{-1}$ results from decomposition, as shown by its irreproducible intensity from different samples and time evolution, due to the extreme air sensitivity of **1**), but the spectrum of **2** (Figure 2b) quite clearly shows the presence of a single component centered at 1786 $cm^{-1}$. Note that the asymmetric unit in the crystal structure of **2** contains only one molecule (one cation and one anion). For both compounds, the band observed in the solid state is closest to the higher frequency band observed in solution.

The two bands have a smaller intensity difference in **2**. Under the assumption of similar extinction coefficients for the Mo−H vibration in the two species, this means that the two species are more equally populated (smaller free energy difference) in **2**. The solution IR spectra recorded at different temperatures (Supporting Information Figures S4 and S5) showed a change of the band intensity ratio, this being more evident for **1** where the Boltzmann population difference is greater. For the neutral complex, an estimation of ca. 0.2 kcal/mol as $\Delta G$ ($G_{minor} - G_{major}$) can be derived from the $I$(1800)/$I$(1730) ratios at the two extreme temperatures: 2.95 at 290 K and 3.5 at 200 K.

The two possibilities envisaged for such equilibrating species are (i) a phosphine ligand dissociation and (ii) a geometric isomerism. To probe for the ligand dissociation hypothesis, spectroscopic studies were carried out in the presence of deliberately added $PMe_3$. The measurement of the intensity ratio of the two IR bands (conditions as in Figure 2, with 10 equiv of $PMe_3$) was prevented by the strong absorption of free $PMe_3$ in the Mo−H stretching region. Useful information, however, could be obtained by NMR and EPR spectroscopy. For the neutral complex, the $^1$H and $^{31}$P NMR spectra of **1**/$PMe_3$ mixtures showed the superposition of the distinct free ligand and hydride complex resonances, demonstrating that ligand exchange between coordinated and free $PMe_3$ is slow on the NMR time scale. Together with the absence of the $^1$H and $^{31}$P NMR resonances of free $PMe_3$ for a solution of pure **1**, this observation rules out the presence of a dissociation equilibrium. Concerning the **2**/$PMe_3$ solutions, the $^1$H and $^{31}$P NMR spectra showed sharp resonances at the usual diamagnetic position for the free $PMe_3$, unaffected by the presence of the paramagnetic complex. Thus, ligand exchange is slow on the NMR time scale also for the cationic complex. The parallel EPR

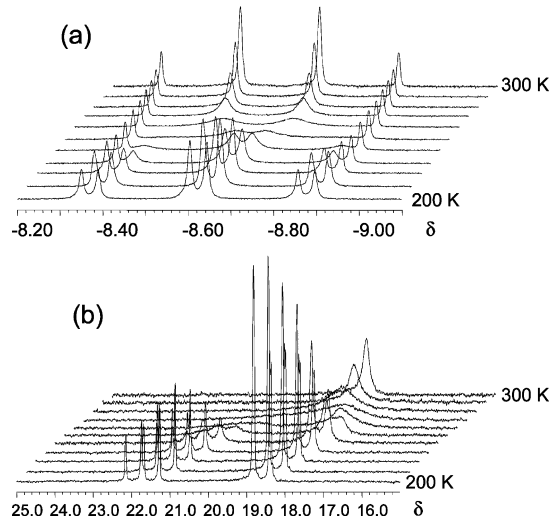


**Figure 3.** Variable-temperature $^1$H (a) and $^{31}$P{$^1$H} (b) NMR properties of the compound Cp*Mo($PMe_3$)$_3$H in toluene-$d_8$. Spectra were taken at 10 K intervals between 200 and 300 K.

investigation shows that the presence of free $PMe_3$ does not alter the line width of the observed resonance. Therefore, no significant $PMe_3$ dissociation is suggested. Hence, we remain with the option of a dynamic process interconverting two different stereoisomers. This possibility was addressed in more detail by DFT calculations (see section d below).

**(c) Low-Temperature NMR Study of Compound 1.** Compound **1** has already been described,[14,21] but its NMR investigation was limited to room temperature, showing a single $^{31}$P resonance and a binomial quartet $^1$H resonance for the hydride signal. This shows that either the three $PMe_3$ ligands occupy symmetry-equivalent positions or a rapid dynamic exchange process is occurring. The peculiar IR spectrum observed for compound **1** has encouraged us to carry out a new NMR investigation at variable temperatures.

The shape of the hydride resonance in the $^1$H NMR spectrum changes upon cooling to ultimately yield a doublet of triplets (Figure 3), demonstrating the presence of a dynamic behavior and two types of inequivalent $PMe_3$ ligands (in a 2:1 ratio) in the ground-state structure. The hydride nucleus has a stronger coupling ($J$ = 77 Hz) with the two equivalent P nuclei and a smaller one ($J$ = 13 Hz) with the unique P nucleus. The two different types of P nuclei are coupled to each other in the low-$T$ $^{31}$P{$^1$H} spectrum with a $J$ of 54 Hz. Simulations with SpinWorks[22] provided an excellent fit, at each temperature, of both $^1$H and $^{31}$P{$^1$H} spectra with the same mutual exchange rate constant (data in the Supporting Information). The Eyring analysis of the temperature-dependent rate constants provided the activation parameters for the mutual exchange: $\Delta H^{\ddagger}$ = 11.7(3) kcal $mol^{-1}$, $\Delta S^{\ddagger}$ = −3(1) eu. The most obvious structure of **1** that fits these data is the four-legged piano stool, identical to that observed by X-ray diffraction for the corresponding cation **2**. We were not successful in growing single crystals of compound **1**, but assuming that the geometry, particularly the bond angles, is not significantly different from that

(21) Shin, J. H.; Parkin, G. *Polyhedron* **1994**, *13*, 1489–1493.
(22) Marat, K. SpinWorks, version 2.5.4. ed., 2006.

observed for **2**, it is interesting to note that the pseudo-*trans* P nucleus shows the weaker coupling and the pseudo-*cis* P nuclei show the stronger one, contrary to the typical situation for *trans* and *cis* arrangements in square planar and octahedral complexes. Stronger coupling in four-legged piano stool geometries between pseudo-*cis* ligands relative to pseudo-*trans* ligands has also been observed in other compounds, notably CpMo(CO)$_2$(PR$_3$)H (R = Me, Ph, Cy)[23−25] and CpOs(P*i*Pr$_3$)H$_3$.[26]

The most interesting observation is the *absence* of any other hydride resonance in the low-temperature spectra. According to the low-temperature IR study (vide supra), a significant amount of the minor isomer (20%) remains present at 200 K, under the assumption that the extinction coefficient for the Mo−H vibration is the same in both species. Since no separate NMR resonance is observed for this isomer, we conclude that the dynamic process that exchanges the major and minor species observed in the IR spectrum is faster than the dynamic process that exchanges the inequivalent PMe$_3$ ligands in the ground-state structure. Furthermore, this dynamic process must maintain the chemical inequivalence of the PMe$_3$ ligands.

The PMe$_3$ exchange process must take place through a more symmetric, higher energy intermediate or transition state. In the case of an intermediate, this is not significantly populated in the temperature range used in our study and is therefore unobserved by IR spectroscopy. The most likely candidate is a pseudotrigonal bipyramidal structure, characterized by *trans* Cp* and H ligands in the axial positions and equivalent PMe$_3$ ligands in the pseudotrigonal plane. As will be shown later in the DFT section, a higher energy local minimum is indeed observed for this geometry. Examples of pseudotrigonal bipyramidal structures for CpML$_4$ complexes are known,[27,28] and the interconversion mechanism between these two geometries has been addressed.[29]

In conclusion, the combined IR and NMR investigation of the compound [Cp*Mo(PMe$_3$)$_3$H] demonstrates that there must be at least three structures in solution: the ground-state structure with inequivalent PMe$_3$ ligands in a 2:1 ratio (presumably a four-legged piano stool), a symmetric intermediate responsible for the mutual PMe$_3$ exchange process (presumably a trigonal bipyramid) that is not thermally populated, and a second asymmetric, thermally populated structure (at ca. 0.2 kcal/mol in enthalpy from the ground state) that exchanges rapidly with the ground-state structure on the NMR time scale, but not on the IR time scale. The nature of these structures has been explored by the DFT calculations.

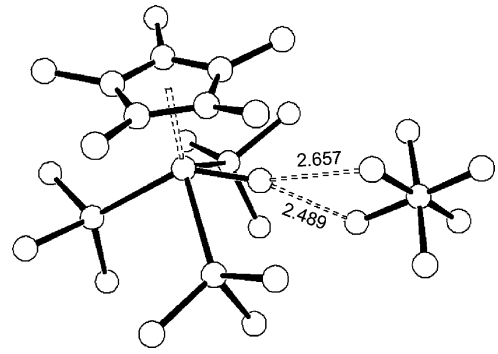


**Figure 4.** Gas-phase optimized geometry of [Cp*Mo(PMe$_3$)$_3$H]PF$_6$. Hydrogen atoms on the Cp* and PMe$_3$ ligands have been omitted for clarity.

**(d) DFT Study of the Ground-State Structures of 1 and 2 and Exchange Barriers.** Geometry optimizations were run for both neutral and cationic complexes, using the systems [(C$_5$R$_5$)Mo(PR′$_3$)$_3$H]$^{n+}$ (*n* = 0, 1), with R = R′ = H (**A**), R = H and R′ = Me (**B**), and R = R′ = Me (**C**, real systems). All optimized geometries, as well as tables of optimized distances and angles, Mo−H stretching frequencies, and a discussion of the structural changes as a function of the chosen model (**A**, **B**, or **C**), are provided as Supporting Information.

The most stable structure was in all cases the typical four-legged piano stool (PS), independent of the model and of the oxidation state. This agrees with our assignment of the observed major $\nu$(Mo−H) band of **1** to the PS isomer. The calculated Mo−H stretching frequencies of **1C**-PS and **2C**-PS (1794 and 1836 cm$^{-1}$, respectively) qualitatively reproduce the experimental trend of a blue shift upon oxidation. The optimized distances and angles for **2C**-PS compare quite well with those experimentally determined by X-ray diffraction (see Table 1), attesting to the suitable level of theory used for the calculations. Comparison of the optimized structures of each redox pair shows interesting trends. The Mo−P distances are longer (by 0.06−0.15 Å) for the oxidized species, whereas the Mo−CNT (ring centroid) and Mo−H distances show a smaller dependence on the metal oxidation state, which is generally in the opposite direction (shorter in the higher oxidation state). These trends cannot be verified experimentally in the absence of an X-ray structure of compound **1**, but were noted recently in the related pair of structurally characterized [($\eta^5$-1,2,4-C$_5$H$_2$*t*Bu$_3$)Mo(PMe$_3$)$_2$H$_3$]$^{n+}$ (*n* = 0, 1) complexes.[12]

Calculations were also run for the ion pair [Cp*Mo(PMe$_3$)$_3$H]$^+$PF$_6^-$ in the gas phase to probe the nature of the cation−anion interaction. The optimized geometric parameters are shown in Table 1. The geometry of the cation is relatively close to that calculated for the isolated cation. The optimization was conducted starting from the relative cation−anion orientation as found in the crystal structure, but the PF$_6$ anion rearranges itself during the optimization procedure to yield two shorter contacts with the hydride ion (Figure 4). These are significantly shorter than in the crystal, suggesting the presence of an attractive force between the hydride ligand and the fluorine atoms of the PF$_6^-$ ion. Indeed, the Mulliken charge calculated for the hydride ligand in **2** is

(23) Kalck, P.; Poilblanc, R. *J. Organomet. Chem.* **1969**, *19*, 115–121.
(24) Faller, J. W.; Anderson, A. S. *J. Am. Chem. Soc.* **1970**, *92*, 5852–5860.
(25) Cheng, T. Y.; Brunschwig, B. S.; Bullock, R. M. *J. Am. Chem. Soc.* **1998**, *120*, 13121–13137.
(26) Baya, M.; Crochet, P.; Esteruelas, M. A.; Gutiérrez-Puebla, E.; Ruiz, N. *Organometallics* **1999**, *18*, 5034–5043.
(27) Du Plooy, K. E.; Moll, U.; Wocadlo, S.; Massa, W.; Okuda, J. *Organometallics* **1995**, *14*, 3129–3131.
(28) Liu, A. H.; Murray, R. C.; Dewan, J. C.; Santarsiero, B. D.; Schrock, R. R. *J. Am. Chem. Soc.* **1987**, *109*, 4282–4291.
(29) Smith, J. M.; Coville, N. J. *Organometallics* **1996**, *15*, 3388–3392.

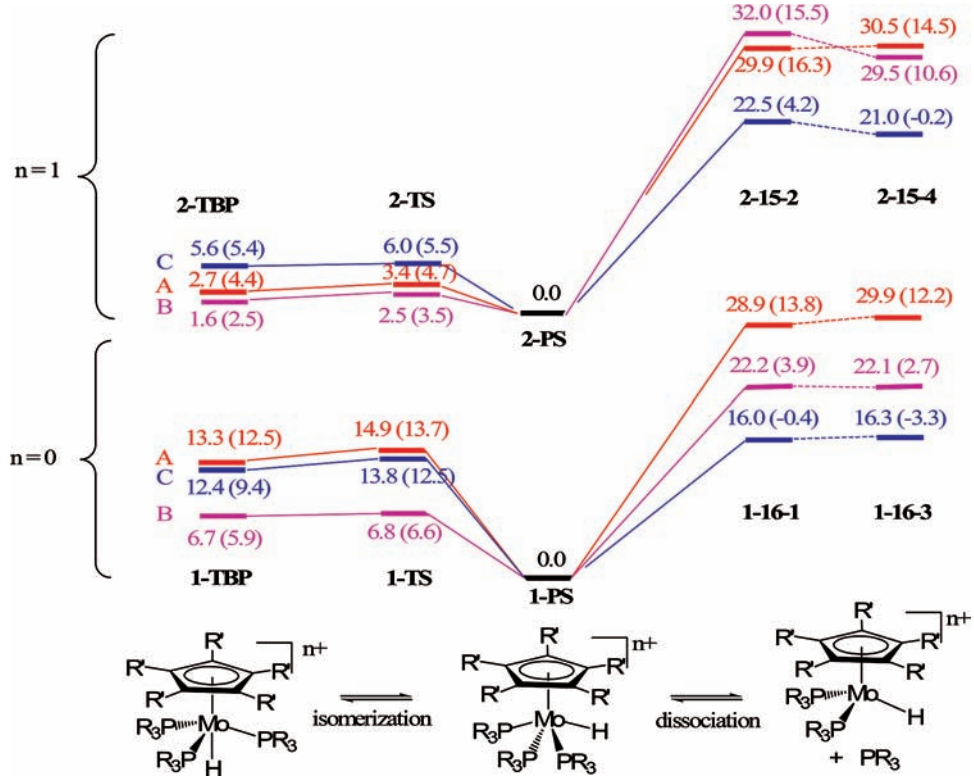


**Figure 5.** Relative energies and gas-phase free energies (in parentheses), kcal mol$^{-1}$, for the isomerization and phosphine dissociation process for models of Cp*Mo(PMe$_3$)$_3$H (bottom) and its one-electron oxidation product (top). The energy values are used to represent the states on the vertical scale. For the definition of the labels **A**, **B**, **C**, **1**, **2**, TBP, TS, 16-1, 16-3, 15-2, and 15-4, see the text.

slightly positive (+0.017), whereas it is negative in **1** (−0.106) and also, although to a lesser extent, in the isolated cation of **2** (−0.066). These Mulliken charge changes confirm the effect of oxidation on the metal−hydride bond polarization and underline the importance of the cation−anion interaction for this polarization. In further support of an attractive force between the hydride ligand and the $PF_6^-$ ion, the related optimization of the adduct of $PF_6^-$ and diamagnetic **1** features much longer H···F separations (2.819, 3.210, and 3.375 Å). The experimentally observed H···F separations in **2** are much longer than the optimized values, possibly because of the effect of neighboring pairs (crystal packing), or because the computational method overestimates the strength of these interactions.

Energy minima corresponding to a pseudotrigonal bipyramidal geometry (TBP), with the hydride and cyclopentadienyl ligands occupying the apical positions, were also located for all model systems in both oxidation states. The geometry with an apical phosphine ligand is unstable and collapses back to the lower energy minimum. We have also optimized the transition state (TS) leading from the ground state PS geometry to the TBP intermediate. The energies for all models, relative to those of the corresponding PS isomer, are visually summarized in Figure 5. Note that the relative energy for **1C**-TS is consistent with the experimentally observed barrier for the mutual $PMe_3$ exchange process ($\Delta H^{\ddagger} = 11.7(3)$ kcal mol$^{-1}$).

In search for a third isomer for **1** and **2**, the energy of which is closer to that of the PS isomer, we have considered the following possibilities: a second minimum along the Berry pseudorotation coordinate (BPR), an agostic cyclopentadiene derivative (AC), a $\sigma$-complex with a C−H bond of a dissociated phosphine ligand (AP), and a Cp rotamer (ROT), as illustrated in Scheme 1. A different minimum in the Berry pseudorotation pathway might be allowed by the presence of two competitive preferred distortions of the ideal PS geometry.[30,31] The AC geometry has previously been proposed and optimized for an intermediate of the isomerization process of the isoelectronic $[Cp^*Fe(dppe)H_2]^+$ complex.[32] The AP geometry, where the dissociated $PMe_3$ ligand

**Scheme 1**

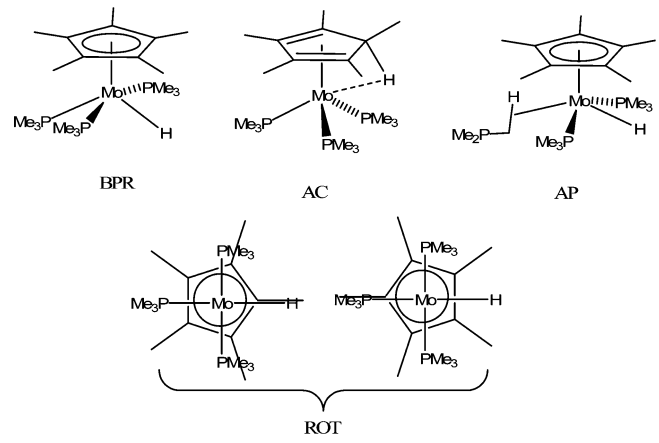


(30) Poli, R. *Organometallics* **1990**, *9*, 1892–1900.
(31) Lin, Z.; Hall, M. B. *Organometallics* **1993**, *12*, 19–23.
(32) Baya, M.; Maresca, O.; Poli, R.; Coppel, Y.; Maseras, F.; Lledós, A.; Belkova, N. V.; Dub, P. A.; Epstein, L. M.; Shubina, E. S. *Inorg. Chem.* **2006**, *45*, 10248–10262.

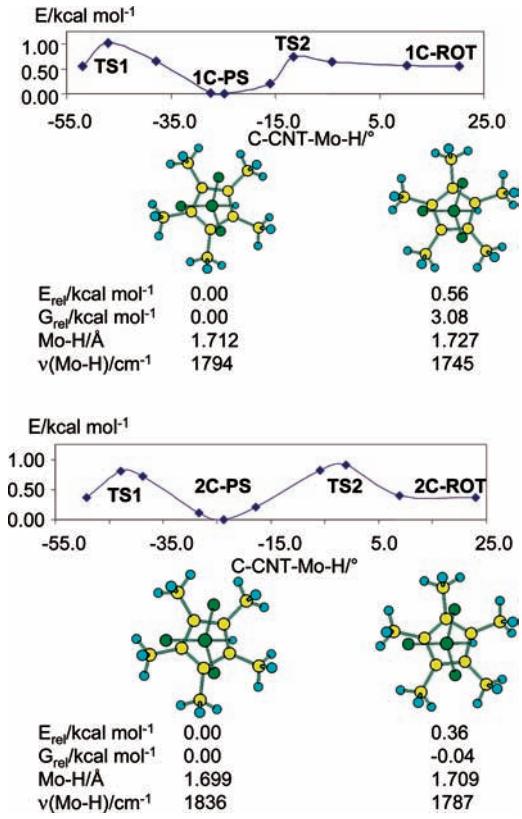


**Figure 6.** Energy of molecules **1C** and **2C** as a function of the C−CNT−Mo−H dihedral angle. Views of the optimized minima emphasizing the Cp* dihedral angle (the $PMe_3$ methyl groups have been removed for clarity) and their calculated Mo−H distances, Mo−H vibrational frequencies, and relative energies and free energies are also shown.

must necessarily be *transoid* to the hydride to maintain the P inequivalence in the low-temperature NMR, may be made energetically favorable by the metal electron richness. Finally, two distinct minima around the Mo−Cp* axis are justified by the symmetry mismatch of the Cp* ring (5-fold) and $ML_4$ moiety (pseudo-4-fold).

The calculations on the BPR, AC, and AP hypotheses show that these cannot rationalize the experimental observation, because either no second minimum could be found or this occurred at a prohibitively high energy (details in the Supporting Information). The hypothesis of a Cp* rotamer, on the other hand, is supported by the computational results. These calculations were carried out only on the full molecule (**C** model). A scan of the energy as a function of the rotation angle is illustrated in Figure 6. The calculations show two minima around the C−CNT−Mo−H dihedral angle, with the second rotamer being located 0.56 kcal mol$^{-1}$ higher in energy (3.08 kcal mol$^{-1}$ in free energy) for **1C**-ROT and 0.36 kcal mol$^{-1}$ higher in energy (but 0.04 kcal mol$^{-1}$ *lower* in free energy) for **2C**-ROT. The highest energy corresponds, for both **1C** and **2C**, to the eclipsed geometry (C−CNT−Mo−H dihedral angle around zero). Note that the calculations reproduce, at least at a qualitative level, the lower energy difference for the two conformers in the cationic complex.

The calculated Mo−H distances and vibrational frequencies are also reported in Figure 6. Notably, the calculated $\nu$(Mo−H) of the global minimum of **1C**-PS is at higher frequency than that of the higher energy minimum, in agreement with the experiment. The calculated frequencies (1794 and 1745 cm$^{-1}$) are also in excellent agreement with the experimental values (1794 and 1730 cm$^{-1}$). For the system **2C**-PS, the calculated frequencies of the nearly isoenergetic rotamers (1836 and 1787 cm$^{-1}$) also compare rather well with the experimentally observed ones (ca. 1800 and 1770 cm$^{-1}$), being blue-shifted relative to the frequencies of the neutral species.

Once likely candidates for the observed species have been found, validation of their independent observation by the IR spectroscopic technique is necessary. First, the calculated rotational barriers shown in Figure 6 are much too low for the individual observation of the rotamers by NMR spectroscopy (for the diamagnetic compound **1**). More typical barriers for processes that can be frozen on the NMR time scale are on the order of 10 kcal mol$^{-1}$, as found above for the P exchange process in **1**. The EPR spectroscopic technique operates on a faster time scale than NMR; fluxional processes with low activation barriers have been investigated by EPR,[33,34] including a substituted cyclopentadienyl ring rotation in the compound $(C_5Ph_4H)Mo(CO)_2(L_2)$ ($L_2$ = 2,3-bis(diphenylphosphino)maleic anhydride) ($\Delta H^{\ddagger}$ = 2.2 kcal mol$^{-1}$).[35] However, the broadness of the EPR resonance of **2** does not permit any coalescence phenomenon to be revealed. Thus, the energy profiles shown in Figure 6 are entirely consistent with the observation of only one species in solution for both **1** and **2** even at low temperatures.

Concerning the IR experiments, in order to observe separate bands for exchanging species with a frequency difference of ca. 60 cm$^{-1}$ (as observed in **1**) or ca. 30 cm$^{-1}$ (as observed in **2**), the exchange rate must be slower than $1.8 \times 10^{12}$ or $9 \times 10^{11}$ s$^{-1}$, respectively, corresponding to activation barriers above 0.7 or 1.1 kcal mol$^{-1}$ according to the Eyring equation. The calculated free energy barriers for the Cp* ring rotation (Figure 6) are indeed higher than these values (3.3 kcal mol$^{-1}$ for **1C** and 1.51 kcal mol$^{-1}$ for **2C**). The smaller frequency difference and the smaller calculated activation barrier for the two rotamers of **2** suggest that the spectrum of this compound is closer to the coalescence region. However, warming this sample to 350 K in dichloroethane shows no clear evidence for the beginning of a coalescence phenomenon (Figure S5, Supporting Information). It should be recalled that the coalescence of IR bands caused by molecular dynamics, though not as familiar as the same phenomenon in NMR spectroscopy, is well established and appreciated.[36−41]

(33) Ittel, S. D.; Krusic, P. J.; Meakin, P. *J. Am. Chem. Soc.* **1978**, *100*, 3264–3266.
(34) Krusic, P. J. *J. Am. Chem. Soc.* **1981**, *103*, 2131–2133.
(35) Mao, F.; Sur, S. K.; Tyler, D. R. *J. Am. Chem. Soc.* **1989**, *111*, 7627–7628.
(36) Macphail, R. A.; Strauss, H. L. *J. Chem. Phys.* **1985**, *82*, 1156–1166.
(37) Wood, K. A.; Strauss, H. L. *J. Phys. Chem.* **1990**, *94*, 5677–5684.
(38) Turner, J. J.; Gordon, C. M.; Howdle, S. M. *J. Phys. Chem.* **1995**, *99*, 17532–17538.
(39) Grevels, F. W.; Kerpen, K.; Klotzbucher, W. E.; Mcclung, R. E. D.; Russell, G.; Viotte, M.; Schaffner, K. *J. Am. Chem. Soc.* **1998**, *120*, 10423–10433.
(40) Londergan, C. H.; Kubiak, C. P. *Chem.—Eur. J.* **2003**, *9*, 5962–5969.
(41) Cahoon, J. F.; Sawyer, K. R.; Schlegel, J. P.; Harris, C. B. *Science* **2008**, *319*, 1820–1823.

The separate observation of different rotamers for these two redox-related compounds is worth a brief discussion because it is unusual. This is apparently the first reported case of the simultaneous IR observation of metal−hydrogen stretching vibrations in different rotamers of a cyclopentadienyl hydride complex. We attribute this observation to the concurrence of a few favorable circumstances. The first one is the highly crowded nature of the molecule, with the $PMe_3$ and Cp* methyl groups imposing relatively large barriers to go past each other through the Cp* ring rotation. The second one is the relatively high frequency difference for the two rotamers, created by a sufficiently different transmission of electronic and steric effects from the Cp* conformation to the Mo−H bond in the two separate minima. In addition to the above factors, we point out that metal−hydrogen stretching vibrations typically have relatively low extinction coefficients, requiring high concentrations (thus high solubility) and long optical paths for measurement of the absorption bands at reasonably high signal to noise ratio (S/N). Thus, this phenomenon may have been missed in previously investigated complexes of this type. Other hydride complexes containing the Cp* ring that have been investigated in our laboratories, for instance, Cp*M(dppe)H (M = Fe,[42] Ru,[43] Os[44]) for which high-quality (high S/N) spectra were obtained, only show a single band, because there is only a single minimum around the M−Cp* rotational coordinate, or because the different minima are related by a lower rotational barrier, or again because the two structures have much closer vibrational frequencies.

Even though the experimental evidence is against the occurrence of $PMe_3$ dissociation, the bisphosphine complexes resulting from the dissociation of one phosphine ligand were also optimized. These are open-shell systems and may adopt two different spin states[45] (singlet and triplet for the 16-electron neutral system, doublet and quartet for the 15-electron cationic one). They are represented by the codes 16-1, 16-3, 15-2 and 15-4, respectively. The relative energies for each system are also shown in Figure 5. Strictly on the basis of energy, the phosphine dissociation is less favorable than isomerization to the TBP structure for both oxidation state levels. If we take into account the entropic contribution, the phosphine dissociation process becomes less disfavored and indeed becomes the preferred process in the gas phase. However, the free energy lowering caused by the entropic contribution in a condensed phase cannot be precisely estimated, because of the partial quenching of the translational and rotational degrees of freedom.

Note that, independent of the model used for the calculation and contrary to the isomerization to TBP, ligand dissociation is more favorable for the neutral system. It should be noted that the phosphine bond dissociation energy is more strongly dependent on the steric bulk than on the oxidation state: it is lowered by 10 kcal $mol^{-1}$ on going from system **A** to system **C** for **1** and by 15 kcal $mol^{-1}$ for **2**, but only by ca. 5 kcal $mol^{-1}$ on going from **1C** to **2C**. Therefore, phosphine dissociation becomes possible for bulkier systems. In this respect, we point out our recent isolation and crystallographic characterization of a salt of $[(1,2,4\text{-}C_5H_2tBu_3)MoH(PMe_3)_2]^+$, though this was obtained by another route ($H_2$ reductive elimination from $[(1,2,4\text{-}C_5H_2tBu_3)MoH_3(PMe_3)_2]^+$).[11,12] Another point of interest is the relatively similar energies for the two possible spin configurations for the dissociation product, both for the neutral and for the cationic systems, independent of the chosen model, the difference being less than 3 kcal $mol^{-1}$. Given the empirical and imprecise handling of electron pairing by density functional methods,[46−50] it is not possible to make reliable predictions as to the spin state adopted by these unsaturated species. The above-mentioned cationic 15-electron system containing the bulkier $1,2,4\text{-}C_5H_2tBu_3$ ligand was found to adopt a spin quartet ground state.[11,12]

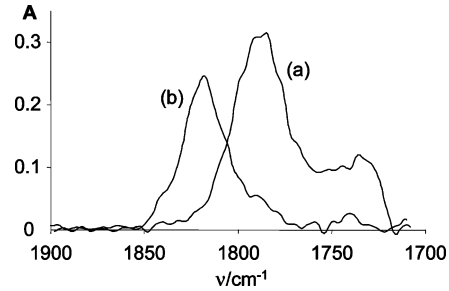


**Figure 7.** Change of the IR spectrum upon protonation in THF at 200 K: (a) $Cp^*Mo(PMe_3)_3H$, (b) $Cp^*Mo(PMe_3)_3H$ in the presence of 1 equiv of $HBF_4$.

**(e) Protonation of $[Cp^*Mo(PMe_3)_3H]$.** Protonation of compound **1** with $HBF_4$ in THF affords the cationic dihydride complex $[Cp^*Mo(PMe_3)_3H_2]^+$, **3** (eq 2). An IR study shows that both $\nu_{MoH}$ bands of **1** disappear, to give rise to only one new high-frequency band at 1818 $cm^{-1}$ (Figure 7).

$$[Cp^*Mo(PMe_3)_3H] + HBF_4 \rightarrow [Cp^*Mo(PMe_3)_3H_2]^+BF_4^- \quad (2)$$

The classical nature of **3** was confirmed by the VT NMR measurements (Figure 8). At 200 K in $CD_2Cl_2$, the complex exhibits two separate $^1H$ resonances in the hydride region with a 1:1 integral ratio (doublet of triplets of small doublets at $\delta$ −3.03 and triplet of small doublets at $\delta$ −6.53) with $T_1$ values (200 K, 500 MHz) of 280 and 330 ms, respectively. The phosphorus atoms in this complex are also nonequivalent at 200 K and appear in the $^{31}P\{^1H\}$ spectrum as a doublet and a triplet at $\delta$ 7.6 and −1.2 ($J_{PP}$ = 23 Hz) with a 2:1 integral ratio. The coupling pattern for the hydride signals was established by a series of $^1H\{sel\ ^{31}P\}$ experiments, as shown in Figure 8. Thus, the two hydrides are coupled to

(42) Belkova, N. V.; Revin, P. O.; Epstein, L. M.; Vorontsov, E. V.; Bakhmutov, V. I.; Shubina, E. S.; Collange, E.; Poli, R. *J. Am. Chem. Soc.* **2003**, *125*, 11106–11115.
(43) Belkova, N. V.; Dub, P. A.; Baya, M.; Houghton, J. *Inorg. Chim. Acta* **2007**, *360*, 149–162.
(44) Dub, P. A.; Belkova, N. V.; Lyssenko, K. A.; Silantyev, G. A.; Epstein, L. M.; Shubina, E. S.; Daran, J.-C.; Poli, R. *Organometallics* **2008**, *27*, 3307–3311.
(45) Poli, R. *J. Organomet. Chem.* **2004**, *689*, 4291–4304.
(46) Salomon, O.; Reiher, M.; Hess, B. A. *J. Chem. Phys.* **2002**, *117*, 4729–4737.
(47) Harvey, J.; Aschi, M. *Faraday Discuss.* **2003**, *124*, 129–143.
(48) Poli, R.; Harvey, J. N. *Chem. Soc. Rev.* **2003**, *32*, 1–8.
(49) Wasbotten, I. H.; Ghosh, A. *Inorg. Chem.* **2007**, *46*, 7890–7898.
(50) Conradie, J.; Ghosh, A. *J. Chem. Theory Comput.* **2007**, *3*, 689–702.

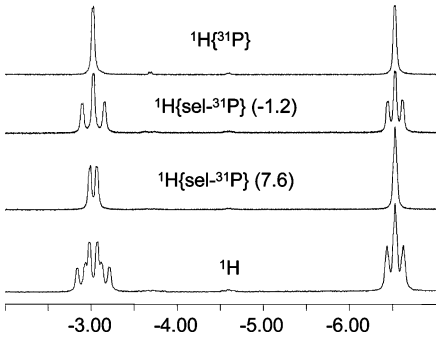


**Figure 8.** Low-temperature (200 K) $^1$H NMR spectra of compound **3** in $CD_2Cl_2$ with various P decoupling modes.

each other with $J_{HH} = 7$ Hz. The hydride at $\delta$ −3.30 shows a stronger coupling ($J_{HP} = 65$ Hz) to the two equivalent P nuclei ($^{31}$P resonance at $\delta$ 7.6) and a weaker one ($J_{HP} = 41$ Hz) to the unique P nucleus ($^{31}$P resonance at $\delta$ −1.2). On the other hand, the hydride at $\delta$ −6.53 is significantly coupled only to the two equivalent P nuclei ($J_{HP} = 45$ Hz), whereas the coupling to the unique P nucleus is not clearly discernible in the $^1$H{sel $^{31}$P: 7.6} spectrum and is estimated as ca. 10 Hz. These data are in agreement with a pseudo-octahedral geometry for **3** in which one of the hydride ligands is *trans* to the Cp* ring, but do not allow unambiguous determination of which resonance belongs to which hydride ligand. However, a comparison of the observed coupling constants of **3** with those found for **1** (where the assignment is unambiguous), and considering the similarity of the bond angles in the optimized structures of the two compounds (vide infra for compound **3**), strongly suggests that the signal at $\delta$ −3.30 should correspond to the axial hydride ligand and that at −6.53 to the equatorial one. A similar structure was reported for the isoelectronic $[CpW(CO)_2(PMe_3)(H)_2]^+$-$[OTf]^-$ compound[51] and later proposed for the related $[CpMoH_2(CO)(dppe)]^+[OTf]^-$ compound.[52] It has also been observed for the isoelectronic molybdenum complex $[CpMo(PMe_3)_3(MeCN)H]^{2+}$ in its $BF_4^-$ salt, where the pseudoequatorial hydride position is replaced by the neutral MeCN molecule.[13]

The $^1$H hydride resonance and the $^{31}$P resonances broaden with the loss of observable coupling upon a temperature increase, showing coalescence at ca. 250 K. Knowledge of the full coupling pattern allowed simulation (Figure 9) and an Eyring analysis of the rate constant for the exchange process (Supporting Information Figure S8). The rate constants for the H and P exchange processes that best fit the experimental data are essentially identical at each temperature, suggesting that the same pathway simultaneously exchanges the two types of nuclei. A least-squares Eyring fit to the data yields $\Delta H^{\ddagger} = 9.3 \pm 0.1$ kcal/mol and $\Delta S^{\ddagger} = -4.1 \pm 0.4$ eu for the hydride exchange process and $\Delta H^{\ddagger} = 9.2 \pm 0.1$ kcal/mol and $\Delta S^{\ddagger} = -4.9 \pm 0.5$ eu for the P exchange process.

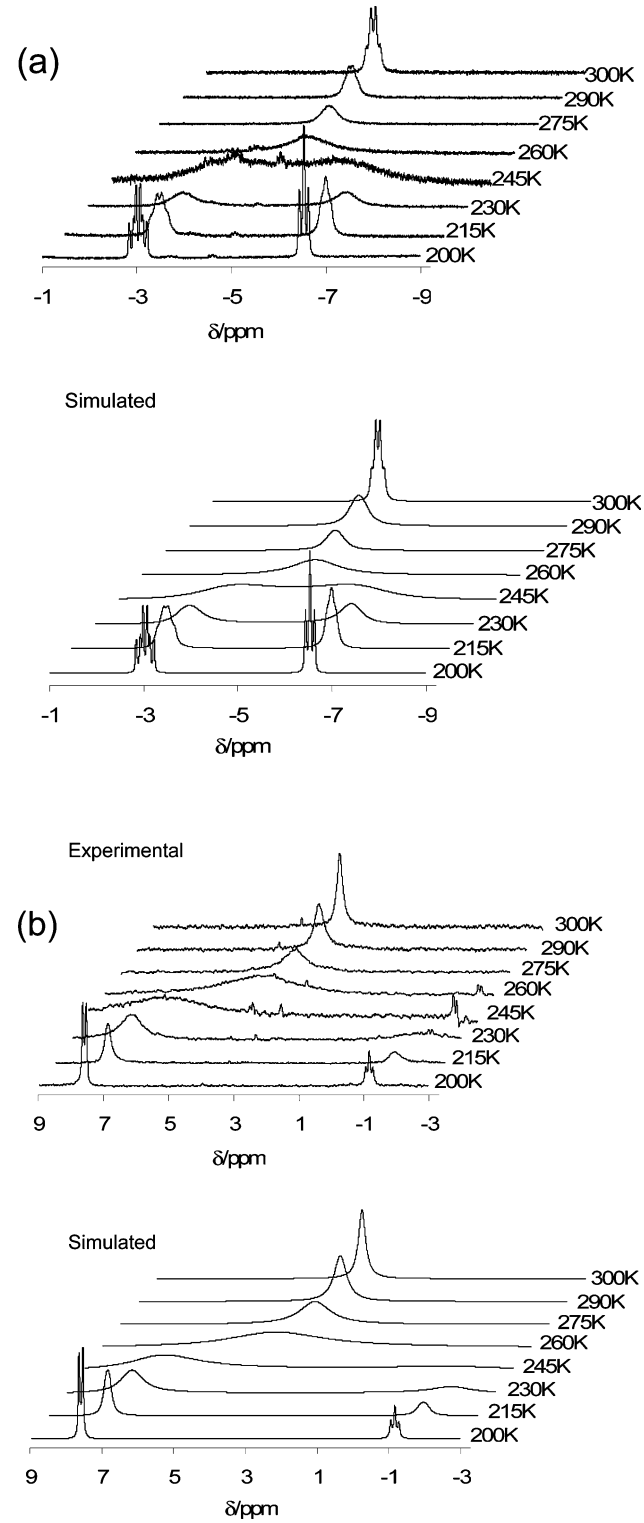


**Figure 9.** Experimental and simulated NMR spectra for compound **3** at various temperatures: (a) $^1$H NMR, (b) $^{31}$P{$^1$H} NMR.

**(f) DFT Study of Compound 3.** Compound **3** has also been subjected to a computational study, with the specific aim to support the proposed ground-state geometry and to identify the likely hydride and phosphine exchange pathway. These calculations were carried out for the full system $[Cp^*Mo(PMe_3)_3H_2]^+$. The results are shown in Figure 10. Three different local minima were found. The global minimum (**3a**) corresponds indeed to the asymmetric pseudo-

(51) Bullock, R. M.; Song, J.-S.; Szalda, D. J. *Organometallics* **1996**, *15*, 2504–2516.
(52) Cheng, T.-Y.; Szalda, D. J.; Zhang, J.; Bullock, R. M. *Inorg. Chem.* **2006**, *45*, 4712–4720.

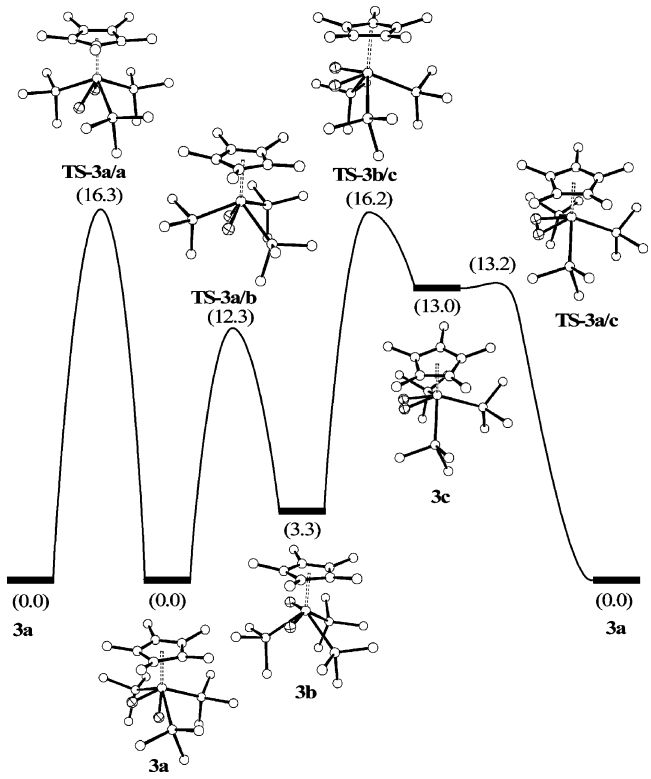


**Figure 10.** Energies (kcal mol$^{-1}$) and geometries of optimized minima and transition states for the system $[Cp^*Mo(PMe_3)_3H_2]^+$.

octahedral structure, with one pseudoaxial (*trans* to Cp) and one pseudoequatorial (*trans* to P) hydride ligand, as suggested by the low-temperature NMR study. A second minimum (**3b**), located 3.3 kcal mol$^{-1}$ higher, also features a classical dihydride structure. This geometry has $C_s$ symmetry, with the two hydride ligands and two $PMe_3$ ligands being symmetry related, while the third $PMe_3$ ligand sits on the mirror plane. The third minimum is a dihydrogen complex with a four-legged piano stool geometry (**3c**), at much higher energy (13 kcal mol$^{-1}$). Four transition states (TSs) interconnecting these minima could be located. As shown in Figure 10, the lowest energy TS is that leading from the global minimum to the symmetric classical isomer, TS-**3a/b**. This rearrangement makes the two H ligands equivalent, and at the same time two previously inequivalent P atoms (one *trans* to the equatorial H atoms and the other one *trans* to the third P atom) become equivalent. Continuation of this process along the opposite and symmetry-related direction exchanges the two H ligands and another pair of P ligands. Thus, this process is in full agreement with the experimental observation of the same activation parameters for the H and P exchange processes. A second exchange mechanism involving the migration of the equatorial hydride to the axial position, thus pushing the axial hydride to the opposite side of the equatorial plane (TS-**3a/a**), is energetically disfavored compared to the previous one. An additional exchange mechanism, whereby the two H ligands exchange their position via rotation of the $H_2$ ligand in a nonclassical isomer, is also not operative in this case, whereas it is rather common for dihydride compounds.[53,54] Not only is the corresponding transition state (TS-**3a/c**) located higher in energy, this mechanism is also excluded because it would not lead to the simultaneous exchange of the P nuclei. This observation emphasizes the strong preference of the classical dihydride structure by this complex.

## Conclusions

By playing on the ligand electron-donating properties and steric bulk, we have managed to produce a thermally stable paramagnetic hydride complex of $Mo^{III}$, $[Cp^*Mo(PMe_3)_3H]^+$. The steric encumbrance of the coordination sphere, in combination with a relatively important effect of the Cp* ring conformation on the Mo−H bond, has allowed the first experimental observation of Cp* distinct rotamers by the IR investigation of a metal−hydrogen stretching vibration. The same phenomenon occurs for the Mo−H stretching vibration of compound **2** and its neutral precursor **1**. Thus, these compounds exhibit dynamic behavior on very different time scales: restricted rotation around the Mo−Cp* axis with barriers in the range of 1 kcal mol$^{-1}$ (picosecond time scale) and hydride ligand mobility with a barrier of 11.7 kcal mol$^{-1}$ (millisecond time scale) for compound **1**. The ligand mobility in compound **2** cannot be probed experimentally, because of the broadness of the EPR resonance.

## Experimental Section

**(a) General Procedures.** All preparations and manipulations were carried out with rigorous exclusion of oxygen and moisture using Schlenk-tube techniques. Solvents were dried by conventional methods and distilled under argon prior to use. The starting material $Cp^*Mo(PMe_3)_3H$ (**1**) was prepared by the published method.[21]

Room-temperature (293 K) NMR investigations were carried out on Bruker DPX300 and Bruker AV300LiQ spectrometers operating at 300.1 MHz ($^1$H), 121.49 MHz ($^{31}$P{$^1$H}), and 75.47 MHz ($^{13}$C{$^1$H}). Low-temperature $^1$H and $^{31}$P data were collected with a Bruker AV500 spectrometer, operating at 500.3 and 202.5 MHz, respectively. The temperature was calibrated using a methanol chemical shift thermometer; the accuracy and stability were ±1 K. All samples were allowed to equilibrate at every temperature for at least 3 min. The spectra were calibrated with the residual solvent resonance relative to TMS ($^1$H, $^{13}$C) and with external 85% $H_3PO_4$ ($^{31}$P). The conventional inversion−recovery−pulse method (180−$\tau$−90) was used to determine the variable-temperature longitudinal relaxation time $T_1$, the calculations being done with standard Bruker software. Coupling constants, $J$, are given in hertz. All NMR simulations were performed with SpinWorks software. VT-EPR spectra were measured on an Elexsys E500 Bruker spectrometer (X-band) equipped with both a frequencemeter and gaussmeter. Cyclic voltammograms were recorded with an EG&G362 potentiostat connected to a Macintosh computer through MacLab hardware/software. The electrochemical cell was fitted with a Ag/AgCl reference electrode, a 1 mm diameter Pt-disk working electrode, and a platinum-wire counter electrode. $[Bu_4N]PF_6$ (ca. 0.15 M) was used as the supporting electrolyte. All potentials are reported relative to the ferrocene/ferrocenium couple. Ferrocene was added and measured as an internal standard at the end of each

(53) Gusev, D. G.; Berke, H. *Chem. Ber.* **1996**, *129*, 1143–1155.
(54) Kubas, G. J. *J. Organomet. Chem.* **2001**, *635*, 37–68.

**Table 2.** Crystal Data and Structure Refinement for [Cp*Mo(PMe$_3$)$_3$]PF$_6$

| | | |
|---|---|---|
| empirical formula | $C_{19}H_{43}F_6MoP_4$ | |
| fw | 605.35 | |
| temp | 180(2) K | |
| wavelength | 0.70930 Å | |
| cryst syst | monoclinic | |
| space group | $P2_1/n$ | |
| unit cell dimensions | $a$ = 9.9347(11) Å | $\alpha$ = 90.0° |
| | $b$ = 15.5051(15) Å | $\beta$ = 90.827(9)° |
| | $c$ = 17.4655(19) Å | $\gamma$ = 90.0° |
| vol | 2690.1(5) Å$^3$ | |
| $Z$ | 4 | |
| density(calcd) | 1.495 Mg/m$^3$ | |
| abs coeff | 0.772 mm$^{-1}$ | |
| $F$(000) | 1252 | |
| cryst size | 0.25 × 0.102 × 0.071 mm$^3$ | |
| $\theta$ range for data collection | 3.08−24.97° | |
| index ranges | $-9 \le h \le +11$, $-18 \le k \le +18$, $-20 \le l \le +20$ | |
| no. of reflns collected | 18043 | |
| no. of independent reflns | 4734 [$R$(int) = 0.0944] | |
| completeness to $\theta$ = 24.97° | 99.8% | |
| abs correction | semiempirical from equivalents | |
| max and min transm | 0.9769 and 0.8497 | |
| refinement method | full-matrix least-squares on $F^2$ | |
| no. of data/restraints/params | 4734/0/290 | |
| goodness-of-fit on $F^2$ | 0.932 | |
| final $R$ indices [$I > 2\sigma(I)$] | R1 = 0.0508, wR2 = 0.1097 | |
| $R$ indices (all data) | R1 = 0.0779, wR2 = 0.1243 | |
| largest diff peak and hole | 0.796 and −0.887 e·Å$^{-3}$ | |

experiment. The solution IR measurements were performed on "Infralum 801" and "Specord M-82" FT-IR spectrometers. Solid-state spectra were measured with a Perkin-Elmer Spectrum 100 FTIR spectrometer (2 cm$^{-1}$ resolution) on the neat solid sample which was pressed inside a quartz crystal. Solution spectra were measured using $CaF_2$ cells of 0.04−0.22 cm path length. All variable-temperature IR measurements in the 190−350 K temperature range were carried out by use of a home-modified cryostat (Carl Zeiss Jena). The cryostat modification allows operation under an inert atmosphere and transfer of the reagents (premixed either at low or room temperature) directly into the cell which is precooled or warmed to the required temperature. The accuracy of the temperature adjustment was ±1 K.

**(b) Preparation of [Cp*Mo(PMe$_3$)$_3$H]PF$_6$ (2).** A suspension of [Cp$_2$Fe]PF$_6$ (60 mg, 0.18 mmol) in tetrahydrofuran (4 mL) was added drop by drop over a cold solution (193 K) of Cp*Mo(PMe$_3$)$_3$H (88 mg, 0.19 mmol) in tetrahydrofuran (4 mL). The solution color gradually changed from green to dark blue and finally to orange in a few minutes. The reaction mixture was warmed to 253 K and then concentrated to ca. 1 mL. Addition of cold diethyl ether (253 K, 8 mL) caused an orange precipitate, which was decanted, washed with cold diethyl ether (253 K, 10 and 8 mL), and vacuum-dried. An orange solid was obtained. Yield: 94 mg (81%). Anal. Calcd for $C_{19}H_{37}F_6MoP_4$: C, 37.70; H, 7.16. Found: C, 38.01; H, 6.85. EPR (X-band, THF): $g$ = 2.014 ($\Delta H_{peak}$ = 22 G) at 110 K; $g$ = 2.011 ($\Delta H_{peak}$ = 180 G) at 253 K. Cyclic voltammetry (THF): $E_{1/2}$ = −0.76 V ($\Delta E_p$ = 123 mV) [ferrocene, $E_{1/2}$ = +0.59 V ($\Delta E_p$ = 318 mV)]. Cyclic voltammetry (MeCN): $E_{1/2}$ = −0.99 V ($\Delta E_p$ = 64 mV) [ferrocene, $E_{1/2}$ = +0.41 V ($\Delta E_p$ = 67 mV)].

**(c) Preparation of [Cp*Mo(PMe$_3$)$_3$H$_2$]BF$_4$ (3).** HBF$_4$ (50%, w/w, in diethyl ether, 30 $\mu$L, 0.20 mmol) was added to a cold solution (273 K) of Cp*Mo(PMe$_3$)$_3$H (89 mg, 0.19 mmol) in diethyl ether (8 mL). Immediate formation of a white solid was witnessed. The suspension was stirred for 10 min and then decanted. The resulting solid was washed with diethyl ether (3 × 10 mL) and dried in vacuo. A white solid was obtained. Yield: 96 mg (82%). Anal. Calcd for $C_{19}H_{44}BF_4MoP_3$: C, 41.63; H, 8.09. Found: C, 41.41; H, 7.94. $^{31}$P{$^1$H} NMR (CDCl$_3$): $\delta$ 4.7 (s). $^1$H NMR (CDCl$_3$): $\delta$ −4.52 (q, $J$ = 49.0 Hz, 2 H, MoH), 1.55 (pseudo-q, $J$ = 2.6 Hz, 27 H, P(CH$_3$)$_3$), 1.96 (s, 15 H, C$_5$(CH$_3$)$_5$). $^1$H NMR (500.3 MHz, CD$_2$Cl$_2$, 200 K): $\delta$ −6.53 (vt, 1H, $J$ = 50 Hz), −3.03 (vdq, 1H), 1.42 (s, 9H, PMe$_3$), 1.47 (s, 18H, PMe$_3$), 1.88 (s, 15H, Cp*). $^{31}$P{$^1$H} (203.5 MHz, CD$_2$Cl$_2$, 200 K): $\delta$ −1.2 (t, 1P, $J$ = 23 Hz), 7.6 (d, 1P, $J$ = 23 Hz). The compound slowly decomposes in CDCl$_3$ and CD$_2$Cl$_2$ at 290 K.

**(d) NMR and EPR Tube Monitoring Experiments.** For all NMR and EPR tube experiments, the sample (ca. 10 mg) was charged as a solid in the glovebox under argon and the tube was sealed with a rubber septum and further wrapped with Parafilm. The solvents and/or other solutions were added to the NMR tube by cannula transfer on a Schlenk line. All solvents were degassed by three freeze−pump−thaw cycles prior to use.

**(e) Computational Details.** Quantum mechanical calculations were performed with the Gaussian03 package[55] at the DFT/B3LYP level.[56−58] Core electrons of the Mo and P atoms were described using the effective core pseudopotentials of Hay−Wadt,[59,60] and valence electrons were described with the standard LANL2DZ basis set.[55] In the case of the P atoms, a set of d-type functions was added.[61] Carbon and hydrogen atoms nonbonded to the metal were described with a 6-31G basis set, carbon atoms linked to the metal were described with a 6-31g* basis set, and the hydride hydrogen atom was described with a 6-31g** basis set.[62−71] All minima and transition states were characterized by analytically computing the Hessian matrix, and no scaling factors were used for the frequencies. Information on atom coordinates (*xyz* files) for all optimized structures is collected in the Supporting Information.

**(f) X-ray Structure Determination.** A single crystal of [Cp*Mo(PMe$_3$)$_3$H]PF$_6$ was mounted under inert perfluoropolyether at the tip of a glass fiber and cooled in the cryostream of an Oxford-Diffraction XCALIBUR CCD diffractometer, and data were collected using monochromatic Mo K$\alpha$ radiation ($\lambda$ = 0.71073 Å). The structure was solved by direct methods (SIR97)[72] and refined by least-squares procedures on $F^2$ using SHELXL-97.[73] All H atoms


(55) Frisch, M. J.; et al. *Gaussian 03*, revision C.02. ed.; Gaussian, Inc.: Wallingford, CT, 2004.
(56) Becke, A. D. *J. Chem. Phys.* **1993**, *98*, 5648–5652.
(57) Perdew, J. P. In *Electronic Structure of Solids*; Ziesche, P., Eschrig, H., Eds.; Akademie Verlag: Berlin, 1991; p 11.
(58) Perdew, J. P.; Wang, Y. *Phys. Rev. B* **1992**, *45*, 13244–13249.
(59) Wadt, W. R.; Hay, P. J. *J. Chem. Phys.* **1985**, *82*, 284–298.
(60) Hay, P. J.; Wadt, W. R. *J. Chem. Phys.* **1985**, *82*, 299–310.
(61) Höllwarth, A.; Bohme, M.; Dapprich, S.; Ehlers, A.; Gobbi, A.; Jonas, V.; Kohler, K.; Stegmann, R.; Veldkamp, A.; Frenking, G. *Chem. Phys. Lett.* **1993**, *208*, 237–40.
(62) Ditchfield, R.; Hehre, W. J.; Pople, J. A. *J. Chem. Phys.* **1971**, *54*, 724–8.
(63) Hehre, W.; Ditchfie, R.; Pople, J. *J. Chem. Phys.* **1972**, *56*, 2257–2261.
(64) Hariharan, P. C.; Pople, J. A. *Mol. Phys.* **1974**, *27*, 209–14.
(65) Gordon, M. S. *Chem. Phys. Lett.* **1980**, *76*, 163–8.
(66) Hariharanan, P.; Pople, J. A. *Theor. Chim. Acta* **1973**, *28*, 213–222.
(67) Blaudeau, J. P.; Mcgrath, M. P.; Curtiss, L. A.; Radom, L. *J. Chem. Phys.* **1997**, *107*, 5016–5021.
(68) Francl, M. M.; Pietro, W. J.; Hehre, W. J.; Binkley, J. S.; Gordon, M. S.; Defrees, D. J.; Pople, J. A. *J. Chem. Phys.* **1982**, *77*, 3654–3665.
(69) Binning, R. C.; Curtiss, L. A. *J. Comput. Chem.* **1990**, *11*, 1206–1216.
(70) Rassolov, V. A.; Pople, J. A.; Ratner, M. A.; Windus, T. L. *J. Chem. Phys.* **1998**, *109*, 1223–1229.
(71) Rassolov, V. A.; Ratner, M. A.; Pople, J. A.; Redfern, P. C.; Curtiss, L. A. *J. Comput. Chem.* **2001**, *22*, 976–984.
(72) Altomare, A.; Burla, M.; Camalli, M.; Cascarano, G.; Giacovazzo, C.; Guagliardi, A.; Moliterni, A.; Polidori, G.; Spagna, R. *J. Appl. Crystallogr.* **1999**, *32*, 115–119.
(73) Sheldrick, G. M. *SHELXL97. Program for Crystal Structure Refinement*; University of Göttingen: Göttingen, Germany, 1997.

attached to carbon were introduced in calculation in idealized positions and treated as riding models. The hydride H atom was located in difference Fourier syntheses and was freely refined with an isotropic thermal parameter. The drawing of the molecule was realized with the help of ORTEP32.[74] Crystal data and refinement parameters are shown in Table 2. Crystallographic data (excluding structure factors) have been deposited with the Cambridge Crystallographic Data Centre as Supplementary Publication No. CCDC 603848. Copies of the data can be obtained free of charge on application to the Director, CCDC, 12 Union Rd., Cambridge CB2 1EZ, U.K. (fax (+44) 1223-336-033, e-mail deposit@ccdc.cam.ac.uk).

**Acknowledgment.** We acknowledge support via bilateral grants (PICS and GDRE "CH2D", France−Russia; LEA, France−Spain) and national support from the Institut Universitaire de France and CNRS (France), the RFBR (Grant 08-03-00464) and the Division of Chemistry and Material Sciences of the Russian Academy of Sciences (Russia), and the Spanish MEC (Project CTQ2005-09000-C02-01 and Consolider Ingenio 2010 CDS2007-00006). M.B. thanks the Spanish Ministerio de Educación y Ciencia for a postdoctoral fellowship and the Spanish MEC/Universidad de Zaragoza for funding through the "Ramón y Cajal" program.

**Supporting Information Available:** Full ref 55, repulsive contacts between the cation and anion in $[Cp^*Mo(PMe_3)_3H]PF_6$, isotropic EPR spectrum and frozen glass spectrum of $[Cp^*Mo(PMe_3)_3H]PF_6$, variable-temperature IR spectrum of $[Cp^*Mo(PMe_3)_3H]$, IR spectra of $[Cp^*Mo(PMe_3)_3H]^+$, mutual exchange rate constants for **1** and Eyring analysis, computational analysis of the BPR, AC, and AP geometries, detailed analysis of structures **A**, **B**, and **C**, Eyring plot of the rate constants derived from the simulation analysis of **3**, and *xyz* coordinates for all optimized geometries. This material is available free of charge via the Internet at http://pubs.acs.org.

IC801676N

(74) Farrugia, L. J. *J. Appl. Crystallogr.* **1997**, *32*, 565.